# A 146.7 GHz Transceiver with 5 GBaud Data Transmission using a Low-Cost Series-Fed Patch Antenna Array through Wirebonding Integration

Arda Simsek[1,2], Seong-Kyun Kim[3], Mohammed Abdelghany[1], Ahmed S. H. Ahmed[1], Ali A. Farid[1], Upamanyu Madhow[1], and Mark J. W. Rodwell[1]

[1]ECE Department, University of California, Santa Barbara, CA, 93106, USA
[2]Movandi, 7555 Irvine Center Dr, Suite 100, Irvine, CA, 92618, USA
[3]Teledyne Scientific and Imaging, 1049 Camino Dos Rios, Thousand Oaks, CA, 91360, USA
ardasimsek@ece.ucsb.edu

***Abstract* — We present a fully-packaged two-channel transmitter and a fully-packaged four-channel receiver using previously reported four-channel transceivers, designed in 45 nm CMOS SOI. We first present a low-cost antenna and packaging technologies to integrate with the transceivers. 8-element series-fed linear microstrip patch antenna arrays fabricated on an Isola Astra MT77 ($\varepsilon_r$=3, tan$\gamma$=0.0017) printed circuit board (PCB) showed 13.6 dB gain, 9º E-plane and 65º H-plane 3-dB beam-widths, and 7 GHz bandwidth (S21), close to simulation. These antennas are connected to CMOS multi-channel transmitter and receiver ICs through wirebonding. Simulations of this interface predict 1.8 dB loss in the IC-antenna ball-bonds (20 µm diameter, 250 µm length) and 0.7 dB loss in the ~1.5 mm PCB microstrip line between the bond pads and the antenna feed point. Using one channel of these transmitter and receiver boards, we demonstrate 5 GBaud BPSK wireless data transmission over 25 cm air with $3x10^{-5}$ bit-error-rate (BER) and 19 dB signal-to-noise-ratio (SNR) at 146.7 GHz carrier frequency.**

***Index Terms* — Millimeter wave integrated circuits, transceivers, transmitters, receivers, CMOS, SOI, phased arrays, MIMO, antennas, wirebonding transition, wireless data transmission.**

## I. Introduction

The rapid increase in data consumption creates a need for high-data-rate wireless links. Millimeter waves provide broad available spectrum, supporting high-data-rate wireless communications. Although ($\lambda^2/R^2$) and foul-weather attenuation are both high, phased arrays can recover the signal strength [1]. Given the short wavelengths, many antennas can be placed in a small aperture area, supporting many independent simultaneous beams (massive MIMO). To realize such complex systems, low-cost, high-yield technologies are critical. For this, CMOS is attractive, and several CMOS transceivers operating above 100 GHz have been previously reported [2, 3].

There is still the need for low-cost yet efficient and high-gain antennas and low-cost assembly techniques at these frequencies. Many published mm-wave systems have used on-chip antennas [4] with limited gain and efficiency, or wafer probing [5] to demonstrate data transmission. Importantly, recent work demonstrated low-loss Cu-stud flip-chip IC - antenna interconnection above 100 GHz [6]. Such assembly provides low IC-package interconnect losses but requires tighter lithographic resolution in the package design.

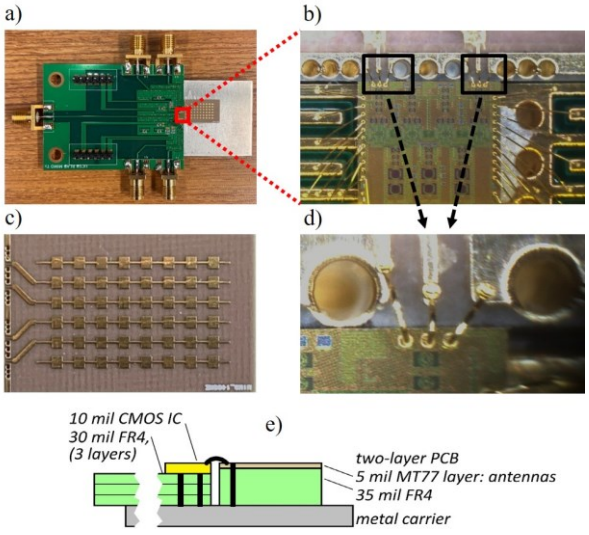


Fig. 1. (a) Two-channel transmitter integrating a CMOS transceiver IC, a PCB carrying a microstrip patch antenna array, and a second PCB carrying low-frequency connections to the IC. (b) Four-channel receiver integrating two CMOS transceiver ICs and antennas (c) PCB 4-element antenna array, each of which is an 8-element series-fed linear microstrip patch antenna array. (d) Magnified image of the wire-bonds. (e) Schematic cross-section of the assembly.

This work presents system-level design and experimental results integrating previously reported [7] 140 GHz CMOS multi-channel transceiver ICs with PCB-based antenna arrays to form a two-channel transmitter and a four-channel receiver. The IC and PCB are connected by simple ball bonds. The antenna array has

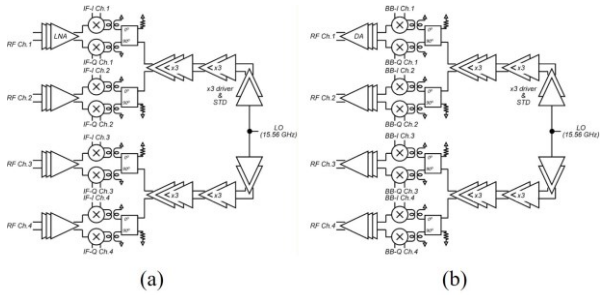


Fig. 2. Schematic diagrams of the four-channel (a) receiver and (b) transmitter

four elements with separate electrical feeds, each element being a series-fed microstrip patch antenna array. The linear array antennas are separated by ~0.5$\lambda$ (1.1 mm) to allow steering over wide angles without grating lobes. We present system and board design, antenna design and measurements, wirebond transition design and simulations at D-band, followed by a BPSK wireless data transmission experiments using one channel of these transmitter and receiver boards.

## II. 4-Channel MIMO Transceivers

The 4-channel transmitter and receiver ICs were previously reported in [7]. They are direct conversion from/to baseband (Fig. 2). Local oscillator (LO) comes through 9:1 frequency multiplier chain from a ~15.5 GHz input. Two such multipliers feed the four channels. Same 140 GHz amplifier is used both in the transmitter and receiver. Only difference is that transmitter uses active Gilbert cell based I/Q modulator, whereas receiver uses passive double-balanced down-conversion mixer. The transmitter saturated output power is -2 dBm with a 1 V supply and 2 dBm with the 1.1 V supply at 145 GHz [7]. The receiver conversion gain is 18 dB with 10-12 GHz 3-dB IF bandwidth [7].

## III. Antenna Design and Measurements

An 8-element 144 GHz series-fed microstrip patch antenna array is designed using a PCB material, Isola Astra-MT77, ($\varepsilon_r$=3, tan$\gamma$=0.0017). The designs are fabricated in a low-cost PCB technology with 3 mil minimum resolution and 5 mil substrate thickness. The PCB is a two-layer laminate with a 35 mil FR4 under the MT77 layer. The combined thickness of the MT77 and FR4 layers is equal to the combined thickness of the CMOS IC and the FR4 board on which it is mounted (Fig.1e). Bond pads on the CMOS IC and on the antenna PCB are therefore at equal height, minimizing wirebond length. Series-fed microstrip patch antenna arrays are

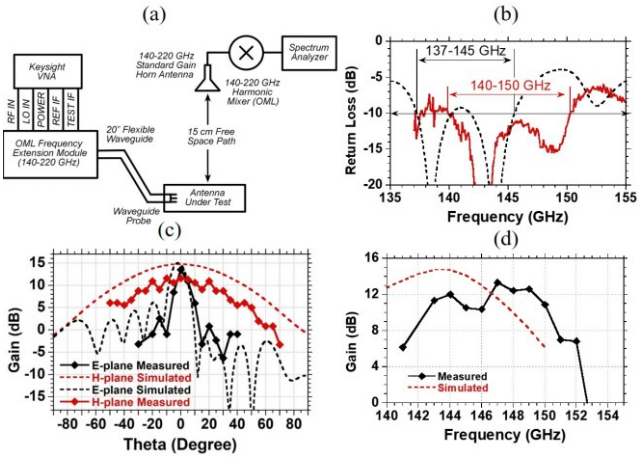


Fig. 3. (a) mm-Wave Antenna measurement setup (b) Simulated and measured return loss of the 144 GHz 8-element series-fed patch antenna array. (c) Simulated (144 GHz) and measured (148 GHz) E-plane and H-plane radiation patterns of the 144 GHz series-fed patch array. (d) Simulated and measured gain vs. frequency curves of the 144 GHz series-fed array.

designed and simulated in Ansys HFSS using the techniques described in [8], with a quarter wavelength transformer matching the antenna array input to 50Ω. Anticipating that simulated and measured antenna resonant frequencies might differ, antennas were fabricated with designed resonant frequencies of 136, 140, and 144 GHz.

Antenna return loss was measured using a mm-wave network analyzer, and radiation patterns were measured using the system of Fig. 3a. In both measurements, the antennas are driven through mm-wave wafer probes. Reported measurements are corrected for probe and instrument losses. Fig. 3b shows the return loss of a single-row 8-element series-fed patch array designed for 144 GHz operation. Defining the antenna bandwidth at the -10 dB return loss points, the measured antenna center frequency is ~4 GHz higher than the simulation, due to the over-etching during the manufacturing. Patterns of this antenna were therefore tested at 148 GHz. Fig. 3c compares the simulated (at 144 GHz) and measured (at 148 GHz) E-plane and H-plane radiation patterns. The peak antenna gain, at ~13.6 dB, is 1.5-2 dB smaller than the simulated. The measured and simulated bandwidth are close to 7 GHz (Fig. 3d).

## IV. Wirebonding Compensation And Transition Design

The wirebond transition between the antenna and the 140 GHz CMOS transceiver RF ports are designed using Ansys HFSS. As noted, board thicknesses are selected such that the height of the antenna and the CMOS pads are

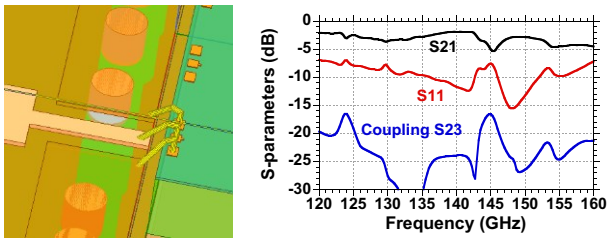


(a) (b)

Fig. 4. (a) Detailed view of the wire-bonded IC-PCB transition in Ansys HFSS including CMOS ground-signal-ground (GSG) pads, GSG ball bonds, grounded coplanar waveguide (GCPW) transmission line, ground vias and edge fringing capacitor at the transition (b) simulated performance, showing insertion loss (S21), return loss (S11) and antenna-antenna coupling (S23).

aligned within +/- 50 µm accuracy (Fig. 4a). In assembly, the gap between the CMOS carrier PCB and the antenna PCB distance is kept below 50 µm (Fig. 1). This permits less than a 0.3 mm wirebond length, giving less than 250-300 pH inductance. The CMOS IC signal pads are ground-signal-ground; hence the antenna PCB substrate provides vias connecting the microstrip ground plane to ground pads which are bonded to the CMOS IC ground pads (Fig 4a). The vias add additional series inductance.

The IC-PCB transition (Fig. 4a) contains a 430 µm length high-impedance (~90Ω) grounded coplanar waveguide transmission line as a series tuning element. The fringing capacitance between the end of the wider 50Ω microstrip line and the CPW ground plane provides shunt tuning. The transition designed in Ansys HFSS (Fig. 4b) shows 1.8 dB loss at 140 GHz for the transition. There is an additional 0.7 dB simulated loss for the 50Ω microstrip line between the IC-PCB transition and the antenna feed point. There is a small gain notch at 145-146 GHz. Isolation between adjacent antenna ports is better than 20 dB over most of the frequency band of interest.

## V. Transceiver Data Transmission Experiments

The transmitter-receiver ICs and antenna arrays were wire-bonded together to form the two-channel transmitter (Fig. 5c) and four-channel receiver (Fig. 5b). There are only two active transmitter channels. However, receiver board uses two ICs and connects to four antenna feeds, consequently it has four active channels. We only used two channels per IC due to the wirebonding density, and the ease of the assembly. We tested the transceiver using one channels of these boards.

First, we separated the transmitter and receiver boards 30 cm apart (Fig. 5a) and performed a gain-frequency measurement. We applied a single tone continuous waveform to I/Q inputs of one channel of the transmitter,

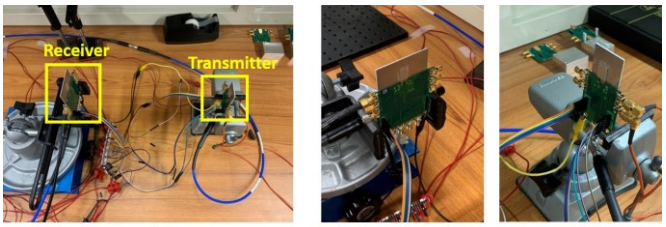


(a) (b) (c)

Fig. 5. (a) Photograph of the experimental setup (b) close view of the 4-channel receiver board (c) close view of the 2-channel transmitter board

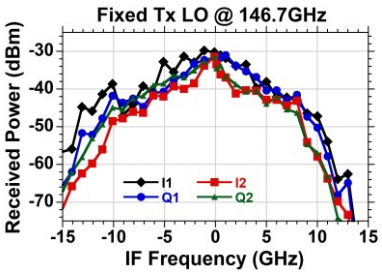


Fig. 6. Received power at 30 cm wireless distance for two different I/Q channels of the receiver board with a fixed LO frequency of 146.7 GHz.

then we measured the received power using spectrum analyzer at the I/Q outputs of the transmitter. We fixed the LO frequency at 146.7 GHz, and swept RF frequency, therefore the IF frequency. We de-embedded the cable losses. At 30 cm wireless distance, received power was measured as ~ -30 dBm, with a ~5 GHz 3-dB IF bandwidth (Fig. 6). Here we reported only two I/Q channels of the receiver, all four channels show similar conversion gain as expected. Using the measurement results together with the IC measurement results [7], wirebonding loss is calculated as ~2.5 dB as shown in equation (1). This is close to the simulations (Loss: free space path loss).

$$P_{sat} + G_{ant,tx} - 2 * WB_{loss} + G_{ant,rx} + G_{Rx} - Loss = P_{rec}$$

$$1 + 13.6 - 2 * WB_{loss} + 13.6 + 12 - 65.3 = -30$$

$$WB_{loss} = 2.45 \text{ dB} \quad (1)$$

We then performed one channel wireless data transmission experiments at 10 cm and 25 cm wireless link (Fig. 5a). Transmitter input was driven by a known data sequence from an arbitrary waveform generator (AWG) with (4096 x 400) symbol length, generated using Matlab. The receiver one channel I/Q outputs were then recorded through a digital oscilloscope (DSAV134A – Keysight). Using Matlab we performed an offline minimum mean square error (MMSE) channel equalization. Both the bit error rate (BER) and signal to

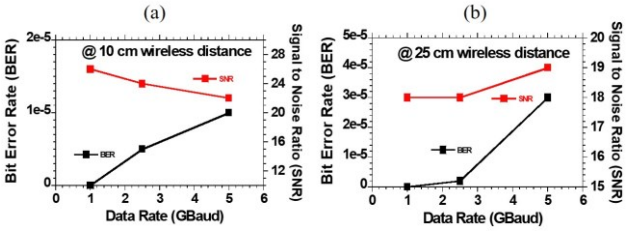


Fig. 7. BER and SNR with respect to data rate with BPSK modulation (a) at 10 cm wireless distance b) at 25 cm wireless distance

noise ratio (SNR) are measured for 1, 2.5, and 5 GBaud data rates. 2.5 and 5 GBaud data rates use an oversampling ratio of 8, whereas 1 GBaud rate uses an oversampling ratio of 10. In this particular experiment, same data streams were sent to I and Q channels (BPSK). Fig. 7 (a) and (b) shows the measurement results at 10 and 25 cm wireless distance respectively. 5 GBaud data transmission rate shows $1x10^{-5}$ BER with 22 dB SNR at 10 cm wireless link (Fig. 7a) and $3x10^{-5}$ BER with 19 dB SNR at 25 cm wireless link (Fig. 7b) using a 146.7 GHz carrier frequency.

BER values are lower than the theoretical values expected for a given SNR for the BPSK modulation. This can be explained by multipath environment as well as the high LO phase noise. In this transceiver IC, LO multiplier chains use an inverter based single-ended to differential converter as a driver circuit for the first tripler. This inverter chain is not immune to the supply noise as well as a transformer coupled interstage network. Therefore, high supply noise can couple to the output through this inverter chain and degrade the LO phase noise. Consequently, this high LO phase noise can explain the lower BER's than the expected BER's with a given SNR at a given modulation scheme.

## VI. Conclusion

We have demonstrated a fully packaged two-channel transmitter and a fully packaged four-channel receiver using low-cost packaging technologies working above 145 GHz. A series-fed linear microstrip patch antenna array exhibits 13.6 dB gain at 148 GHz. Simulated losses of a ball-bonded IC-PCB interface are only 1.8 dB, closed to the calculations from the measurements. One channel of the fully packaged transmitter and receiver boards is used to demonstrate wireless data transmission at 5 GBaud. We obtain $1x10^{-5}$ BER with 22 dB SNR at 10 cm range, and $3x10^{-5}$ BER with 19 dB SNR at 25 cm range.

Packaging is modular and can be extended to realize arrays with larger size, which allows a longer system range. In addition, this system can be further investigated using separate transmit boards to send separate transmit streams to realize true MIMO communications in a multipath environment. This can increase the system data rate drastically compared to the single beam communications.

## Acknowledgement

This work was supported by National Science Foundation (NSF) GigaNets Program, Contract NO. CNS-1518812. The author would like to thank Global Foundries for the 45 nm CMOS SOI chip fabrication, and Advotech for the assembly. Authors also would like to thank Navneet Sharma, Hamidreza Memerzadeh, Nikolaus Klammer and Gary Xu at Samsung Research America for valuable suggestions and the measurement equipment. Authors also would like to thank Prof. James F. Buckwalter for valuable comments.

## References

[1] S. Shahramian, M. J. Holyoak, and Y. Baeyens, "A 16-Element W-Band phased array transceiver chipset with flip-chip PCB integrated antennas for multi-gigabit data links," in Proc. Radio Freq. Integr. Circuits Symp., 2015, pp. 27-30.

[2] A. A. Farid, A. Simsek, A. S. H. Ahmed and M. J. W. Rodwell, "A Broadband Direct Conversion Transmitter/Receiver at D-band Using CMOS 22nm FDSOI," *2019 IEEE Radio Frequency Integrated Circuits Symposium (RFIC)*, Boston, MA, USA, 2019, pp. 135-138.

[3] S. Kang, S. V. Thyagarajan and A. M. Niknejad, "A 240 GHz Fully Integrated Wideband QPSK Transmitter in 65 nm CMOS," in *IEEE J. of Solid-State Circuits*, vol. 50, no. 10, pp. 2256-2267, Oct. 2015.

[4] A. Visweswaran et al., "9.4 A 145GHz FMCW-Radar Transceiver in 28nm CMOS," 2019 IEEE International Solid-State Circuits Conference - (ISSCC), San Francisco, CA, USA, 2019, pp. 168-170.

[5] S. Carpenter et al., "A D-Band 48-Gbit/s 64-QAM/QPSK Direct-Conversion I/Q Transceiver Chipset," in *IEEE Trans. Microw. Theory Tech.*, vol. 64, no. 4, pp. 1285-1296, April 2016.

[6] M. Sawaby, N. Dolatsha, B. Grave, C. Chen and A. Arbabian, "A Fully Packaged 130-GHz QPSK Transmitter With an Integrated PRBS Generator," in *IEEE Solid-State Circuits Letters*, vol. 1, no. 7, pp. 166-169, July 2018.

[7] A. Simsek, S. Kim and M. J. W. Rodwell, "A 140 GHz MIMO Transceiver in 45 nm SOI CMOS," 2018 IEEE BiCMOS and Compound Semiconductor Integrated Circuits and Technology Symposium (BCICTS), San Diego, CA, 2018, pp. 231-234.

[8] B. Rupakula, A. Nafe, S. Zihir, Y. Wang, T. Lin and G. Rebeiz, "63.5–65.5-GHz Transmit/Receive Phased-Array Communication Link With 0.5–2 Gb/s at 100–800 m and ± 50° Scan Angles," in *IEEE Transactions on Microwave Theory and Techniques*, vol. 66, no. 9, pp. 4108-4120, Sept. 2018.